

A Microfluidic Reactor for Enhancing Electrochemical Water Splitting

Tong Shi^{1,2}, Hao Feng^{2,*}, Dong Liu², Ying Zhang², Qiang Li^{2,*}

¹ School of Energy and Power Engineering, Xi'an Jiaotong University, Xi'an 710049, China

² School of Energy and Power Engineering, Nanjing University of Science and Technology, Nanjing 210094, China

*Corresponding author: fenghao@njust.edu.cn (Hao Feng); liqiang@njust.edu.cn (Qiang Li)

ABSTRACT

Electrochemical hydrogen gas evolution on the electrode surface will occupy the limited active sites thus significantly increases the reaction overpotential. It is crucial to study and optimize the bubble behavior on the electrode surface to improve the reaction efficiency and lower the energy loss. Herein, a microfluidic electrochemical reactor (MER) was constructed to optimize the surface kinetic behavior during the gas evolution process. The obtained results demonstrate the feasibility of microfluidic design in manipulating the bubble behavior at the electrode interface through the self-generated gas-liquid two-phase flow, which can simultaneously reduce the overpotential and facilitate the mass transfer. Compared with the traditional H-cell, the hydrogen evolution efficiency can present a remarkable intensification. Our work reveals a new strategy for guiding the design of the electrochemical reactor for water splitting.

Keywords: Electrochemical water splitting; Microfluidic reactor; Mass transfer; Two-phase flow; Bubble behavior.

1. INTRODUCTION

Water electrolysis is considered an effective way to develop sustainable and environmentally friendly hydrogen energy^[1]. From the perspective of overall electrochemical water splitting, the processes of gaseous product evolution, including nucleation, growth, desorption, coalescence, etc. are slower in time scale than reactant adsorption and electron migration. This mismatch results in the occupation of active sites thus the increase in ionic resistance and the great energy loss^[2]. Meanwhile, the large adhesion force associated

with the large bubble desorption will lead to the loss of catalyst loading, resulting in irreversible current loss^[3]. Hence, it is of great significance to regulate the kinetic behavior of bubbles on the electrode surface.

Most researches have focused on designing catalysts with better performance and lower cost^[4,5], but reducing kinetic impedance is equally important. At present, the designs of the surface structure of the catalyst have been proved to be beneficial to promote bubble desorption^[6,7]. However, these improvement measures are only limited to the design of catalytic electrodes.

The transfer process of matter on the electrode surface is vital and usually described by the Nernst-Planck equation:

$$J_i(x) = -D_i \frac{\partial c_i(x)}{\partial x} - \frac{z_i F}{RT} D_i c_i \frac{\partial \varphi(x)}{\partial x} + c_i v(x)$$

the right side of the equation represents the diffusion term, the electromigration term, and the convection term in electrochemical process. Diffusion migration and electromigration are closely related to the characteristics of carriers in reaction, while convective migration is closely related to the bubble behavior on the electrode surface. In general, it is hard to remove bubbles timely by buoyancy or simple stirring. For this reason, a microfluidic electrochemical reactor was designed for manipulating the interface bubble behavior by enhancing convection. It provides a new idea for further improvement of water electrolytic efficiency by inducing forced convection and forming various flow patterns in designing electrode.

2. METHODS

2.1 Reactor design and assembly

The schematic of the reactor is shown in Fig. 1, where

Selection and peer-review under responsibility of the scientific committee of the 13th Int. Conf. on Applied Energy (ICAE2021).

Copyright © 2021 ICAE

the catalyst is loaded on the sidewall of electrode plate channel. The electrolyte is circulating, and the liquid inlet flow rate can be adjusted by the peristaltic pump to obtain different gas-liquid two-phase flow patterns in the flow channel. Besides, a typical H-cell was also fabricated for comparison.

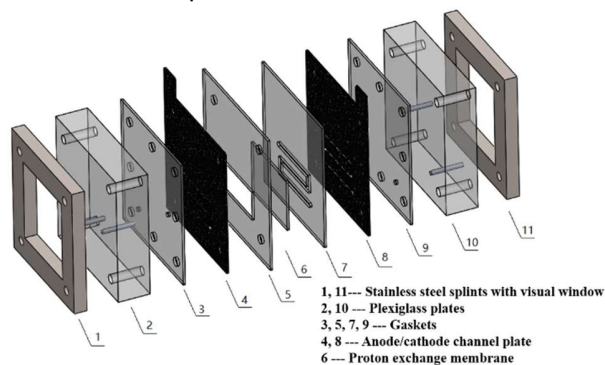


Fig. 1 Assembly diagram of MER.

2.2 Preparation of catalyst

To emphasize the optimization driving by changing bubble behavior, commercial catalysts Pt/C (20 wt%) and IrO₂ were used as Hydrogen/Oxygen Evolution Reaction (HER)/(OER) catalysts in this work. For the cathode preparation, the Pt/C was firstly dispersed in isopropanol and then sprayed onto the sidewall of microchannel flow plate. Then, the sample was dried at 80°C. The final loading was controlled at 0.2 mg/cm² Pt/C. The same procedure was utilized for the anode preparation.

2.3 Test conditions and electrochemical test methods

The test was operated under room temperature and atmospheric pressure. All electrochemical tests were performed at CHI 660E electrochemical workstation. The electrochemical active surface area (ECSA) tests were carried out by selecting a sweeping range from 0.59 V to 0.69 V as the non-Faraday region. Electrochemical impedance spectroscopy (EIS) was performed in the range of 100 kHz to 1 Hz. The scan rate of linear sweep voltammetry (LSV) was carried out at 0.1 V/s, and the flow rate was set as 5 ml/min in MER. All I-T curves were measured under two-electrodes system, and all the tests under different conditions were carried out on the same corresponding carbon paper plate / microchannel electrode.

3. RESULTS AND DISCUSSION

Some characteristics of electrodes and the reactors are shown in Fig. 2. First of all, due to the peculiarities of the preparation process for each electrode, the disparities in catalyst loading were inevitable. Hence, it is

necessary to carry out ECSA tests on the prepared electrodes. We performed CV tests with different sweeping rates in the non-Faraday potential range, and calculated the double-layer capacitance (C_{dl}) to emerge the ECSA. As shown in Fig. 2a, it can be seen that the C_{dl} of carbon paper electrode is 5.54 mF/cm², slightly larger than the 4.36 mF/cm² of microchannel electrode, which indirectly shows the difference in ECSA of the two electrodes. This also serves as a reference for a more objective comparison of subsequent electrochemical test differences between two electrodes, especially the difference in current density. In addition, the advantage of MER in internal resistance is obvious. The difference between MER and H-cell in EIS performance is shown in Fig. 2b. It can be seen that the ohmic internal resistance (R_i) of MER is lower than that of the H-cell. This is partly due to the integrated characteristics of the MER, which combines the flow channel plate (reaction chamber), catalyst, and current collector. Moreover, MER shorts the distance between anode and cathode. The properties result in less energy loss especially under high current working conditions, resulting in the reactor having more potential for industrial application.

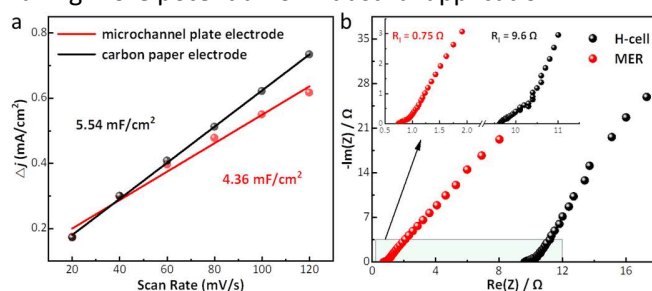


Fig. 2 a) The capacitance of double electric layer (corresponding to ECSA) of microchannel plate and carbon paper electrodes, b) EIS performance of MER and H-cell.

To directly obtain the current density improvement brought by the optimized bubble behavior during reaction process, we tested the I-T curves with five different flow rates (0.2 ml/min, 0.5 ml/min, 1 ml/min, 2 ml/min and 5 ml/min) in MER under a constant voltage of -2V. The results shown in Fig. 3b revealed that the current density increases in response to the gradual increase of liquid flow rate. Comparing the two flow rate conditions of 0.2 ml/min and 5 ml/min, the average catalytic current density increased from -95 mA/cm² to -165 mA/cm², a conspicuous gain of 70 mA/cm² was obtained by improving the kinetics and mass transfer process of bubbles on the catalytic surface. At the end of the test in MER, we adjusted the flow rates back to previous, the current almost returned to same levels.

This further indicated that the enhancement was due to the better mass transfer effect.

In addition, it is noteworthy that the current fluctuation at high flow rate is much lower than at low flow rate. This is because the current fluctuation is mainly related to the average desorption time of gaseous products. A longer desorption time corresponds to a longer occupation time and more occupied sites, so the impedance extreme value at the react site is larger and the current fluctuation is more apparent. In this way, this phenomenon corresponds to a smaller average desorption size and a shorter average desorption time of the bubbles at higher flow rates.

As shown in Fig. 3, the LSV curves of the two reactors have significant differences. It is worth mentioning that even though the ECSA of the electrode in MER is slightly smaller than H-cell, the MER can achieve a higher current response at a lower cell potential. According to the steady-state I-T test in Fig. 3b, the average current density of MER increases from -26 mA/cm^2 of H-cell to -95 mA/cm^2 even though the MER operates at a low flow rate. Moreover, the current density corresponding to the flow rate of 5 ml/min in the MER reached -165 mA/cm^2 , which was a remarkable improvement of nearly 140 mA/cm^2 . This also demonstrated the significance of improving the key rate-limiting step of bubble behavior. It is an important section to break through the existing energy conversion efficiency of electrolytic water.

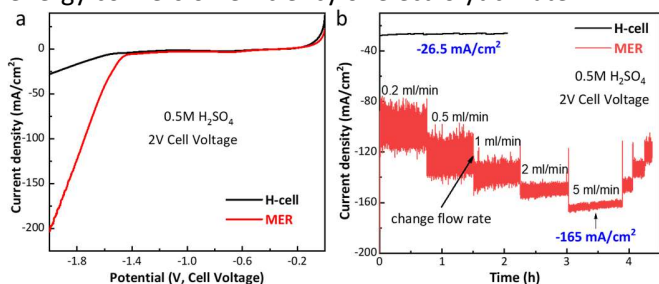


Fig. 3 a) LSV and b) I-t curves corresponding to different reactors at -2 V constant potential, in which the curve of MER includes the current response of different flow rates.

Visual states corresponding to different flow rates were carried out to clearly analyze the mass transfer enhancement of the reactor. Figs. 4a-4c show the flow patterns correspond to the flow rates of 0.2 ml/min , 1 ml/min , and 5 ml/min , respectively. At a low flow rate of 0.2 ml/min , due to the small shear force, the bubbles could not be quickly separated from the solid catalyst surface, so the gaseous products gradually coalescent into larger bubbles. Then, such large bubbles coalesce again in the subsequent flow channel and become slug, flowing through rest of the subsequent flow channel wall

surface. The long slugs make liquid reactant exist only in the form of thin liquid film on wall surface loaded catalysts, and the resulting thin liquid film enables bubbles generated in these regions to be swallowed by slug at a smaller critical bubble size in the earlier formation process and then flow away. As the small bubbles continuously coalesced into the gas slugs, the elongated slug flow was finally formed as shown in Fig. 4a. However, the disadvantage is that the reactant supply of the liquid film is limited. When the flow rate increases to 1 ml/min , it can be observed that the slug length is shortened and the number of slugs is increased, which means that the bubbles in the subsequent passages also form slugs independently under stronger shear forces and more immediate reactant supply. When the velocity of up to 5 ml/min , the flow pattern changes from slug flow to bubble flow. The rapid separation behavior of bubbles prevents them from coalescence in the subsequent flow process so that the active sites are constantly released and refreshed under the shear force brought by strong flow, thus reducing occupied time and intensifying reactant supply. Therefore, the optimization is significantly better than slug flow.

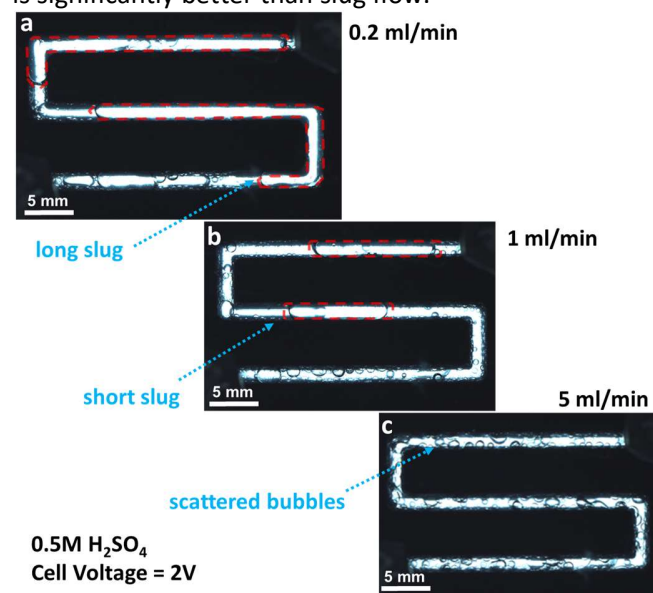


Fig. 4 Visual images of the gas-liquid two-phase flow in MER at different liquid flow rates.

It can be seen that although the slug flow in flow channel plays a role in thinning the liquid boundary layer on the catalyst surface at low flow rates, its optimization effect is not as good as the mass transfer optimization brought by strong shear force at high flow rates. The greater surface shear stress applied by forced convection, the smaller bubble desorption size, and the better reactant supply. For different catalytic systems,

such as different catalyst loads (number of active sites), electrolyte and working potentials, there is a critical limit forced convection rate matching them, which makes the steps in the catalytic process as coupled as possible for the relatively optimal operating conditions.

Finally, we made a comparative analysis with the existing research data under similar test conditions [8-10], and the results are listed in Fig. 5. For the same test conditions in Refs. 8 and 10, the LSV performances are nearly the same. By comprehensive comparison of catalyst type and loading, test conditions, and LSV results, the MER can achieve better catalytic performance in the acidic electrolyte at room temperature and atmospheric pressure with lower catalyst loading, due to its advantages such as reducing system internal ohmic resistance, kinetics and mass transfer overpotential by bubble behavior optimization.

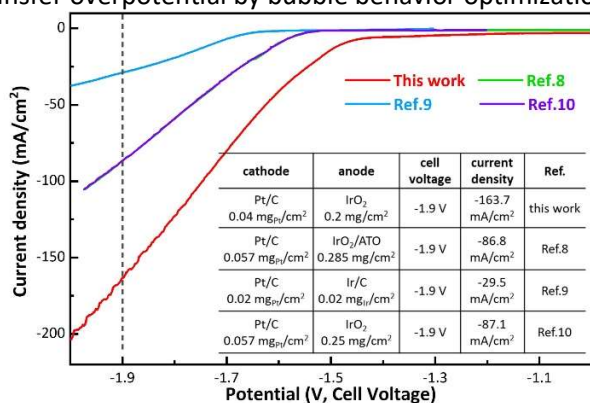


Fig. 5 Comparison of LSV performance between the present study and previous works.

4. CONCLUSION

In this work, a microfluidic electrochemical reactor was constructed to optimize the interface behavior during bubbles evolution process. The self-forming and controllable two-phase flow was realized during the reaction in MER. Different flow patterns corresponding to different flow rates bring diverse optimizations. In addition to make reactor more compact, microchannel electrode organically combines catalyst, current collector, and reaction chamber also reduced the ohmic loss in MER. Therefore, MER offers the possibility for high current operation applications. Compared with H-cell, the current density of the MER at high flow rate of 5 ml/min brings an excellent improvement of nearly 5.4 times (from -26 mA/cm² to -165 mA/cm²). The MER greatly optimizes the kinetics and mass transfer sections in the process of water electrolysis by reducing the bubble desorption size and providing sufficient supply of reactants through introducing forced convection

shearing and forming different flow patterns. It provides a new design idea and solution for further improving the water electrolysis efficiency.

ACKNOWLEDGEMENT

This work was supported by the National Natural Science Foundation of China (Nos. 52006101, 52006103, 51888103), Natural Science Foundation of Jiangsu (BK20200491), and Fundamental Research Funds of the Central Universities (No. 30920021137).

REFERENCE

- [1] Xue S, Liu Z, Ma C, Cheng HM, Ren WJSB. A highly active and durable electrocatalyst for large current density hydrogen evolution reaction. *Sci Bull* 2020;65:123-30.
- [2] Kou T, Wang S, Li Y. Perspective on high-rate alkaline water splitting. *ACS Mater Lett* 2021;3:224-34.
- [3] Song Q, Xue Z, Liu C, Qiao X, Liu L, Huang C, Liu K, Li X, Lu Z, Wang T. General strategy to optimize gas evolution reaction via assembled striped-pattern superlattices. *J Am Chem Soc.* 2020;142:1857-63.
- [4] Zheng T, Shang C, He Z, Wang X, Cao C, Li H, Si R, Pan B, Zhou S, Zeng J. Intercalated iridium diselenide electrocatalysts for efficient pH-universal water splitting. *Angew Chem Int Edit* 2019;58:14764-9.
- [5] Dou S, Li X, Wang X. Rational design of metal-organic frameworks towards efficient electrocatalysis. *ACS Mater Lett* 2020;2:1251-67.
- [6] Zhang Q, Xiao W, Guo W, Yang Y, Lei J, Luo H, Li N. Macroporous array induced multiscale modulation at the surface/interface of Co(OH)₂/NiMo self-supporting electrode for effective overall water splitting. *Adv Funct Mater* 2021;31:2102117.
- [7] Kou T, Wang S, Shi R, Zhang T, Chiovoloni S, Lu J, Chen W, Worsely MA, Wood BC, Baker SE, Duoss EB, Wu R, Zhu C, Li Y. Periodic porous 3D electrodes mitigate gas bubble traffic during alkaline water electrolysis at high current densities. *Adv Energy Mater* 2020;10:2002955.
- [8] Luo F, Hu H, Zhao X, Yang Z, Zhang Q, Xu J, Kaneko T, Yoshida Y, Zhu C, Cai W. Robust and stable acidic overall water splitting on Ir single atoms. *Nano Lett.* 2020;20:2120-8.
- [9] You H, Wu D, Chen Z, Sun F, Zhang H, Chen Z, Cao M, Zhuang W, Cao R. Highly active and stable water splitting in acidic media using a bifunctional iridium/cucurbit[6]uril catalyst. *ACS Energy Lett* 2019;4:1301-7.
- [10] Hu H, Kazim FMD, Ye Z, Xie Y, Zhang Q, Qu K, Xu J, Cai W, Xiao S, Yang Z. Electronically delocalized Ir enables efficient and stable acidic water splitting. *J Mater Chem A* 2020;8:20168-74.